

We are IntechOpen, the world's leading publisher of Open Access books Built by scientists, for scientists

5,500

Open access books available

136,000

International authors and editors

170M

Downloads

Our authors are among the

154

Countries delivered to

TOP 1%

most cited scientists

12.2%

Contributors from top 500 universities



WEB OF SCIENCE™

Selection of our books indexed in the Book Citation Index
in Web of Science™ Core Collection (BKCI)

Interested in publishing with us?
Contact book.department@intechopen.com

Numbers displayed above are based on latest data collected.
For more information visit www.intechopen.com



Current Status and Prospects of Solid-State Batteries as the Future of Energy Storage

Marm Dixit, Nitin Muralidharan, Anand Parejiya, Ruhul Amin, Rachid Essehli and Ilias Belharouak

Abstract

Solid-state battery (SSB) is the new avenue for achieving safe and high energy density energy storage in both conventional but also niche applications. Such batteries employ a solid electrolyte unlike the modern-day liquid electrolyte-based lithium-ion batteries and thus facilitate the use of high-capacity lithium metal anodes thereby achieving high energy densities. Despite this promise, practical realization and commercial adoption of solid-state batteries remain a challenge due to the underlying material and cell level issues that needs to be overcome. This chapter thus covers the specific challenges, design principles and performance improvement strategies pertaining to the cathode, solid electrolyte and anode used in solid state batteries. Perspectives and outlook on specific applications that can benefit from the successful implementation of solid-state battery systems are also discussed. Overall, this chapter highlights the potential of solid-state batteries for successful commercial deployment in next generation energy storage systems.

Keywords: solid electrolyte, composite cathode, lithium-ion, batteries, lithium anode

1. Introduction

The dawn of the 21st century coincided with the global civilization leapfrogging into the digital age. At the core of this digital revolution was the rapid adoption and wide deployment of lithium-ion batteries (LIBs) [1]. Ever since, both industries and the scientific community have been engaged in the quest for unlocking the secrets for developing batteries with more energy, -power, -life, and -safety. In the recent years, the battery R&D community is once again at the cusp of another technological revolution that could redefine the energy storage sector for decades to come. This revolution is largely fueled by the rapidly advancing efforts into a new battery technology called all Solid-State Batteries (ASSBs) [2]. While conventional lithium-ion batteries have enjoyed unprecedented levels of research and industrial attention directed towards every aspect of their constituents, SSBs have largely been on the backburner. For decades, the battery research sector has been constantly attempting to integrate high-capacity lithium metal anodes (3860 mAh.g^{-1}) to advance energy density targets of liquid electrolyte-based LIBs[3]. However, in such conventional batteries, the hydrocarbon derived organic liquid electrolytes

pose significant safety and performance related challenges with lithium metal anodes and has also been a significant barrier preventing wide commercial deployment [4]. With renewables and electric vehicles (EV) set to dictate the timeline for the next industrial revolution, the battery R&D community has come to a profound consensus that conventional lithium-ion batteries are nearing their upper limits of performance [5]. The initial interest towards SSBs was based on the use of solid electrolytes (SE), as they are potentially thought to provide a straightforward approach towards realizing the safe integration of high-energy lithium metal anodes. In recent years, new classes of high-performance solid electrolytes have emerged with high room-temperature conductivities ($\sim 1 \text{ mS}\cdot\text{cm}^{-1}$) [6] comparable to that of conventional liquid electrolytes and high lithium-ion transference numbers (~ 1 for inorganic SE) [7]. This coupled with novel processing approaches targeting interfacial tuning and optimizations are propelling the new generation of SSB systems towards garnering a widespread support for commercial adoption. With the EV demand projected to skyrocket in the next few years, the need for the next-generation high energy batteries that would power these advanced automotive platforms is also growing [1, 8–10]. To this extent, several large-cap automotive companies including Toyota, Volkswagen, General Motors, Hyundai, and Ford have already made major investments in SSB technology companies with the aim to achieve full commercial deployment in the first half of the 21st century.

Despite the optimism and promises around all SSBs, there are several major challenges pertaining to each cell component and processing approach that needs further optimizations to achieve the overarching performance goals. For SSBs, there can be several material-level issues that can cause major cell-level catastrophic failures. We had recently reported that an ideal solid-state battery (**Figure 1a**) that delivers a high energy density should consist of the following [11] – (i) a high-capacity thin lithium metal anode/seed layer (thickness $\sim 1\text{-}5 \mu\text{m}$ seed layer + $15\text{-}40 \mu\text{m}$ plated from the cathode), (ii) a stable solid electrolyte with high ionic conductivities (thickness $\sim 1\text{-}20 \mu\text{m}$, ideally dry), (iii) a cathode composite with optimized loading and tailored architecture (thickness $\sim 45\text{-}200 \mu\text{m}$) [12]. In order to achieve high energy densities in SSBs, it is generally understood that the cathode should be the most voluminous part. Current collectors employed in an SSB can generally be $< 10 \mu\text{m}$ thick applied in the form of thin coatings to mechanically robust electrodes [13]. Additionally, SSBs also offer the possibility of cell stacking in two different configurations depending upon performance requirements – conventional stacking and bipolar stacking [14]. Bipolar stacking in a single package using bipolar current collectors decreases the packing volume thus increasing the volumetric energy

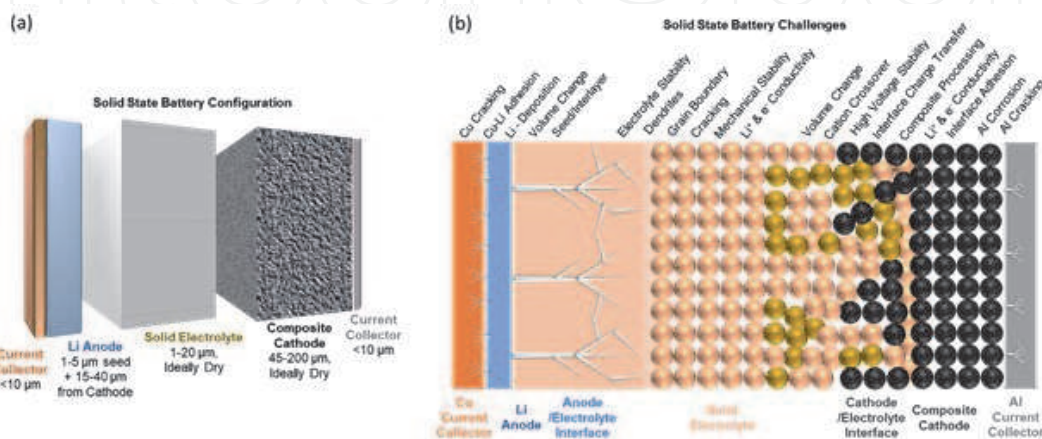


Figure 1.

(a) An ideal solid-state battery with optimized configuration and (b) remaining material level challenges in solid state batteries.

density. Though, the requirements to achieve high performance SSBs appear quite straight forward, significant fundamental issues and challenges pertaining to specific cell components remain unresolved in the SSB R&D space. **Figure 1b** depicts a schematic providing a brief overview of some underlying challenges that warrants systematic investigations and mitigation strategies to enable the wide commercial deployment of SSBs. From the aforementioned figure, it should be noted that interfacial properties play a dominant role in determining the final performance delivered by SSBs [15, 16]. For example, if we consider the simple interface between the anode and the copper current collector, some of the challenges encountered may include (i) current collector corrosion/cracking – due to the repeated mechanical cycling stresses and Li plating related side reactions, (ii) Cu-Li adhesion – improper adhesion between these dissimilar metals can occur due to oxide layer formation during processing or due to cyclic mechanical and electrochemical loads during charge/discharge, (iii) volume change – drastic volumetric expansion/contraction can occur during charge/discharge processes at the anode interfaces owing to the soft and pliable nature of Li metal, etc. Similarly, other interfaces between the lithium metal anode and solid electrolyte, solid electrolyte and cathode composite, cathode composite and positive current collector also suffer from interface related issues which can hamper final cell performance. Additionally, the component specific bulk property variations could also be crucial factors that affect SSB performance and thus demands systematic investigations leading to strategic solutions prior to commercial adoption.

In this chapter, we discuss the critical challenges, recent advances, and avenues for improvement for the various classes of cathodes, solid electrolytes and anodes that would facilitate the commercial adoption of next generation SSBs. We also discuss the key processing and fabrication criteria for assembling full SSBs cells with our recent modelling endeavors into achieving practical cell level energy densities. Finally, we discuss some perspectives on the challenges that remain unsolved as well as the future trends in SSB development. Through this chapter, we envision, the readers would get a comprehensive understanding of the recent trends, remaining challenges, and a clear perspective of the future prospects of all Solid-State Battery R&D.

2. Cathode materials for SSB

The cathode materials play a pivotal role in the energy density, power density, cycle life, and calendar life of a battery. Oxide-based lithium-ion intercalation materials are the cathode of today's choice and can mainly be segregated into five board classes based on their crystal structure.

- i. Spinel structure ($\text{Li}[\text{M}]_2\text{O}_4$ with $\text{M} = \text{Mn}, (\text{Mn}_{1-y/2}\text{Li}_{y/2})$ or $(\text{Mn}_{3/4}\text{Ni}_{1/4})$),
- ii. Layered structure ($\text{Li}[\text{M}]\text{O}_2$ with $\text{M} = \text{Co}, \text{Ni}, (\text{Ni}_x\text{Co}_{1-x})$ or $(\text{Ni}_x\text{Mn}_y\text{Co}_z)$),
- iii. Olivine structure $\text{Li}[\text{M}']\text{PO}_4$ with $\text{M}' = \text{Fe}, \text{Mn}, \text{Ni}, \text{Co}$ or $(\text{Fe}_y\text{Mn}_{1-y})$,
- iv. β II - $\text{Li}_2\text{FeSiO}_4$,
- v. Tavorite-type LiFeSO_4F ,

Apart from these, sulfur and some organic compounds are also used as cathode materials in batteries. Every cathode material and its crystal structure have inherent

advantages and disadvantages from the standpoint of electrochemical energy storage. The basic concept of battery intercalation chemistry is very old [17]. The first intercalation reactions involving solid hosts (graphite) and guest molecules or ions (sulfate ions) were shown by Schaufautl in 1841. However, in the 1960s, the intercalation materials gained attention due to the altering of their electronic and optical properties through guest ion intercalation [18–20]. The transition-metal disulfides and oxides (such as MS_2 and WO_3) were first investigated for intercalation of H^+ , Li^+ and Na^+ ions [17]. It was noted that the intercalation of these monovalent ions into the crystal structure of WO_3 altered the electronic structure and conductivity, resulting in the material changing from an insulator to metal depending upon the amount and types of monovalent cation intercalated. These intercalation reactions were also accompanied by structural changes with modifications to crystal chemistry [21].

2.1. Crystal structure cathode materials

The lattice atom and its coordination domain are the basic structural unit of a crystal. The lattice atoms are arranged periodically in specific combinations (e. g. space group) for the formation of crystals. It should be noted that, in general, the electronic structure and interaction for the bond formation energy in the structure unit ultimately determines the intrinsic chemical and physical properties of crystals [22]. For lithium-ion and sodium-ion batteries, the cathode materials can be formed by combinations of Li, Na, transition metal, and anion structure units. It should be further noted that the crystal structure and chemical composition of the cathode materials play an important role in the ionic and electronic transport properties and conduction mechanisms. The five different crystal structures of cathode materials are displayed in **Figure 2** [23]. The layered structure cathode exhibits two-dimensional ionic and electronic conductivity and diffusivity (**Figure 2a**).

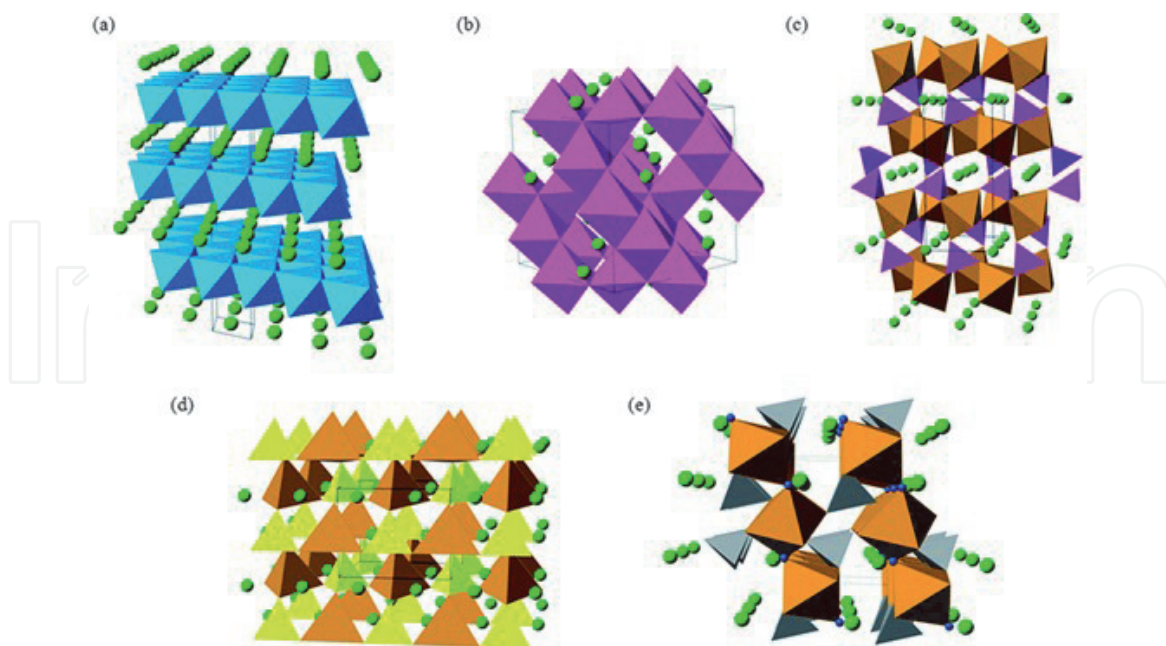


Figure 2.

The crystal structures of major cathode materials: (a) layered α - $LiCoO_2$; (b) cubic $LiMn_2O_4$ spinel; (c) olivine-structured $LiFePO_4$; (d) β II - Li_2FeSiO_4 ; and (e) tavorite-type $LiFeSO_4F$. Li ions are shown as light green spheres, CoO_6 octahedra in blue, MnO_6 octahedra in mauve, Fe–O polyhedra in brown, PO_4 tetrahedra in purple, SiO_4 tetrahedra in yellow, SO_4 tetrahedra in gray, and in (e) fluoride ions in dark blue. Black lines demarcate one unit cell in each structure. (Reprinted with permission from Ref [23]. Copyright 2014, published by The Royal Society of Chemistry. This image is taken from the article titled “Lithium and sodium battery cathode materials: computational insights into voltage, diffusion and nanostructural properties”, and it is under the Creative Commons Attribution 3.0 International License. To view a copy of this license, visit <https://creativecommons.org/licenses/by/3.0/>).

On the other hand, materials belonging to the spinel structure demonstrate three-dimensional ionic and electronic conductivity and ionic diffusivity (**Figure 2b**). In contrast, the olivine structure cathodes showcase preferably one-dimensional ionic conductivity and diffusivity and two-dimensional electronic conductivity (**Figure 2c**). The β II - $\text{Li}_2\text{FeSiO}_4$ and tavorite-type LiFeSO_4F structures (**Figure 2d** and **e**) are not vigorously used in the lithium-ion battery cathode. The layer and spinel structure cathodes exhibit an interstitial type of mechanism of ionic conductivity and diffusivity. The olivine structure materials display vacancy migration type ionic conductivity and diffusivity. Unlike conventional lithium-ion battery (with liquid electrolyte), all solid-state battery (SSB) is impacted by dimensional conductivity, material hardness and mechanical properties which will be discussed in detail in the later sections.

2.2. Electronic and ionic transport properties

In a solid active cathode particle, the ion and electron moving together when charging or discharging the battery and this phenomenon is called ambipolar diffusion. Therefore, optimum ionic and electronic transport properties are prerequisites for high performances batteries, particularly SSBs. Nonetheless, it is very rare to get such good combinations in the presently available list of cathode materials. Some of the reported electronic and ionic conductivity and ionic diffusivity of spinel, layer, and olivine structure materials are compared and displayed in **Figure 3** and **Table 1** as a function of inverse temperature and lithium concentration, respectively.

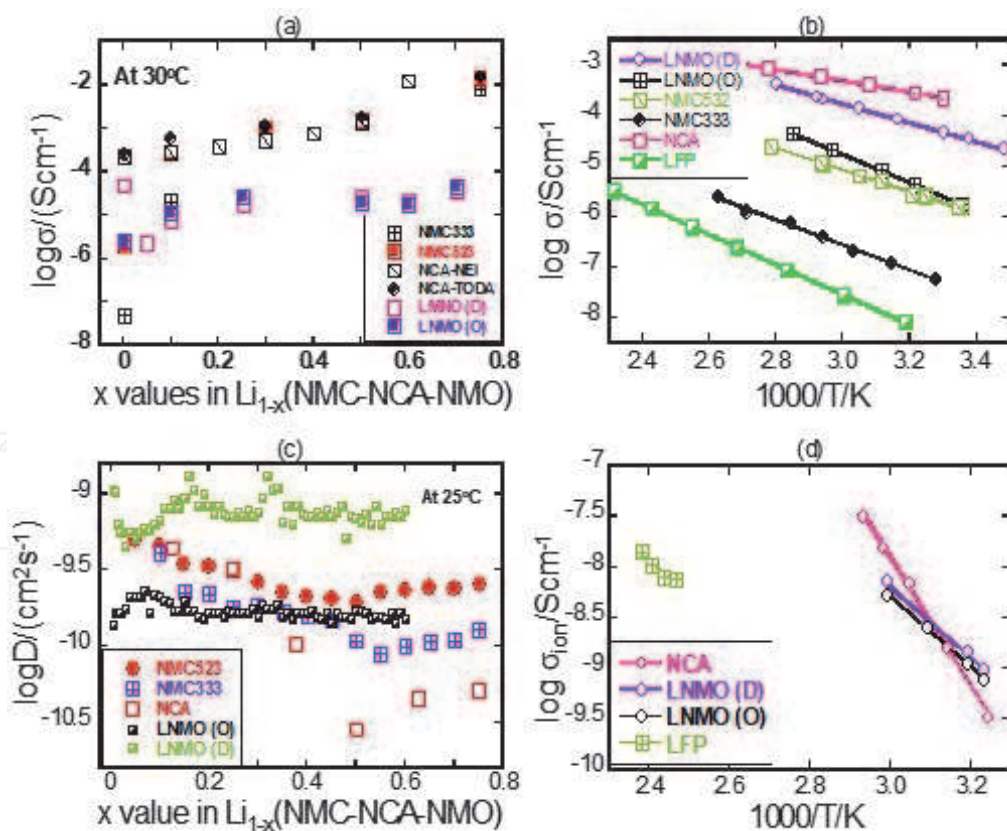


Figure 3.

(a) Electronic conductivity of layer and spinel structure cathodes as a function lithium content, (b) Electronic conductivity of layer, spinel, and olivine structure cathode materials as a function of inverse temperature, (c) ionic diffusivity of layer and spinel structure cathode as a function of lithium content and (d) ionic conductivity of layer, spinel, and olivine structure cathode materials as a function of inverse temperature. $\text{LiFePO}_4 = \text{LFP}$, $\text{LiNi}_x\text{Mn}_y\text{Co}_z\text{O}_2 = \text{NMC}$, $\text{LiNi}_{0.75}\text{Co}_{0.25}\text{Al}_{0.05}\text{O}_2 = \text{NCA}$, $\text{LiMn}_{1.5}\text{Ni}_{0.5}\text{O}_4 = \text{LMNO (O)}$, and $\text{LiMn}_{1.5}\text{Ni}_{0.5}\text{O}_{4-\delta} = \text{LNMO (D)}$. Each of the figures, a, b c and d were made by authors from the following references. [24] = LFP, [25] = (NMC333, NMC523), [26] = (NCA-NEI, NCA-TODA), [27] = (LNMO (O), LNMO (D)), [28] = (LNMO (O), LNMO (D)).

Technique Used	T/°C	Composition	Diffusivity (cm ² /s)	Reference	Structure
AC	60	LiNi _{0.5} Mn _{0.2} Co _{0.3} O ₂ (NMC ₅₂₃)	~3×10 ⁻⁸	[25]	
AC	61	LiNi _{0.33} Mn _{0.33} Co _{0.33} O ₂ (NMC ₃₃₃)	~5×10 ⁻⁸	[25]	
DC	50	LiNi _{0.33} Mn _{0.33} Co _{0.33} O ₂ (NMC ₃₃₃)	~7×10 ⁻⁹	[25]	
Depolarization	25	Li _{0.9} Ni _{0.33} Mn _{0.33} Co _{0.33} O ₂ (NMC ₃₃₃)	~4×10 ⁻¹⁰	[25]	
Depolarization	25	Li _{0.25} Ni _{0.33} Mn _{0.33} Co _{0.33} O ₂ (NMC ₃₃₃)	~10 ⁻¹⁰	[25]	Layer
Depolarization	25	Li _{0.9} Ni _{0.5} Mn _{0.2} Co _{0.3} O ₂ (NMC ₅₂₃)	~5×10 ⁻¹⁰	[25]	
Depolarization	25	Li _{0.25} Ni _{0.5} Mn _{0.2} Co _{0.3} O ₂ (NMC ₅₂₃)	~2×10 ⁻¹⁰	[25]	
GITT	25	LiNi _{0.33} Mn _{0.33} Co _{0.33} O ₂ (NMC ₃₃₃)	~10 ⁻¹¹	[29]	
GITT	25	Li _{0.25} Ni _{0.33} Mn _{0.33} Co _{0.33} O ₂ (NMC ₃₃₃)	~10 ⁻¹⁰	[29]	
GITT	25	LiNi _{0.33} Mn _{0.33} Co _{0.33} O ₂ (NMC ₃₃₃)	~10 ⁻⁹	[30]	
GITT	25	Li _{0.25} Ni _{0.33} Mn _{0.33} Co _{0.33} O ₂ (NMC ₃₃₃)	~5×10 ⁻¹⁰	[30]	
CV	25	LiNi _{0.33} Mn _{0.33} Co _{0.33} O ₂ (NMC ₃₃₃)	~5×10 ⁻¹⁴	[31]	
CV	25	LiNi _{0.33} Mn _{0.33} Co _{0.33} O ₂ (NMC ₃₃₃)	~3×10 ⁻¹⁰	[32]	
AC	25	LiNi _{0.8} Co _{0.15} Al _{0.05} O ₂ (NCA)	~3×10 ⁻¹⁰	[26]	
DC Polarization	25	LiNi _{0.8} Co _{0.15} Al _{0.05} O ₂ (NCA)	~2×10 ⁻¹⁰	[26]	
GITT	25	Li _{0.875} Ni _{0.8} Co _{0.15} Al _{0.05} O ₂ (NCA)	~4×10 ⁻¹⁰	[26]	
GITT	25	Li _{0.9} Ni _{0.5} Co _{0.5} O ₂ (NC)	~10 ⁻¹⁰	[33]	
GITT	25	Li _{0.9} Ni _{0.8} Co _{0.2} O ₂ (NC)	~10 ⁻⁸	[34]	
First principle	25	LiMn _{1.5} Ni _{0.5} O _{4-δ} (LMNO (O))	~10 ⁻⁹	[35]	
DC	50	LiMnO _{4-δ} (LMNO (D))	~8×10 ⁻⁹	[27, 28]	Spinel
AC	25	LiMn _{1.5} Ni _{0.5} O _{4-δ} (LMNO (D))	~5.1×10 ⁻¹⁰	[27, 28]	
GITT	25	LiMn _{1.5} Ni _{0.5} O _{4-δ} (LMNO (O))	~5×10 ⁻¹⁰	[36]	
PITT	25	LiMn _{1.5} Ni _{0.5} O _{4-δ} (LMNO (O))	5×10 ⁻¹² -9 × 10 ⁻¹⁰	[37]	
EIS	25	LiMnO _{4-δ} (LMNO (D))	2.97×10 ⁻¹⁵	[38]	
PITT, EIS	25	LiMn _{1.5} Ni _{0.5} O _{4-δ} (LMNO (O))	10 ⁻¹² -10 ⁻¹⁰	[39]	
DC	147	LiFePO ₄	1.6×10 ⁻⁹	[24]	Olivine

Table 1. Comparison of ionic diffusivity of the selected major classes of cathode materials at specific temperature.

It is seen from **Figure 3a** that the electronic conductivity of spinel (LMNO) and layer structure (NMC and NCA) cathodes show the discrete pattern of conductivity as a function of lithium content. It is discernible from **Figure 3b** that the layer structure materials exhibit a gradual increase of conductivity with increasing degree of delithiation. On the other hand, the electronic conductivity of the spinel structure can be manipulated by varying the degree of disorder and degree of delithiation. It should be noted that the spinel phase exhibits two crystallographic polymorphs, ordered and disordered depending on the distribution of Ni and Mn in the crystal structure. The ordered LiMn_{1.5}Ni_{0.5}O₄ (LMNO (O)) exhibit approximately fifteen times lower electronic conductivity than the disordered LiMn_{1.5}Ni_{0.5}O_{4-δ} (LMNO (D)) phase (**Figure 3a**) in the lithiated states. Also, the electronic conductivities of the ordered spinel LNMO (O), measured at a given

temperature, increases gradually with increasing the degree of delithiation (**Figure 3a**). However, when $x = 0.3$ and beyond, the conductivity is almost leveled where it hardly changes with the removal of lithium in the measured range. It appears that partial lithium off-stoichiometric phases are favorable for better high-rate performances from comparing electronic conductivities for layered and ordered spinel cathodes. In disparity, the electronic conductivity of the disordered spinel (LNMO (D)) is reduced suddenly upon slight delithiation and falls to the level of the electronic conductivity demonstrated by lithiated ordered spinel phase.

Following which, the electronic conductivity exhibits alike trends for both the ordered and disordered phases (**Figure 3a**). The electronic conductivity of the olivine phase as a function of lithium concentration is not available in the literature. However, the electronic conductivity of olivine phase LiFePO_4 exhibits the lowest conductivity as a function of temperature (**Figure 3b**) and layer structure NCA shows the highest conductivity. The ionic conductivity and diffusivity of spinel phases appear to be favorable from the SSB standpoint compared to layered and olivine structure cathodes (cf. **Figure 3c** and **d** and **Table 1**).

2.3. Electrochemical performances and particle morphology

The energy and power density are important metrics to determine the scope of a specific application for cathode materials[35–39]. The theoretical and experimentally obtained capacity, operational average cell voltage (against carbon electrode), and energy density of major cathode materials are compared in **Table 2**. It is discernible from **Table 2** that all the phases of a particular crystal structure belonging to the same material family do not deliver the same energy density. The layer structure cathodes exhibit higher capacity compared to the spinel and olivine.

Crystal structure	Composition	Capacity/mAh/g (theoretical/experimental)	Average cell voltage (V)	Experimental energy density (Wh/kg)	References
Layered	LiTiS_2	225/210	1.9	399	[40]
	LiCoO_2	274/148	3.8	562	[41]
	LiNiO_2	275/150	3.8	570	[42]
	LiMnO_2	285/140	3.3	462	[43]
	$\text{LiNi}_{0.33}\text{Mn}_{0.33}\text{Co}_{0.33}\text{O}_2$	280/160	3.7	592	[44]
	$\text{LiNi}_{0.8}\text{Co}_{0.15}\text{Al}_{0.05}\text{O}_2$	279/199	3.7	736	[45]
	Li_2MnO_3	458/180	3.8	684	[46]
Spinel	LiMn_2O_4	148/120	4.0	480	[47]
	$\text{LiMn}_{1.5}\text{Ni}_{0.5}\text{O}_4$	148/140	4.1	574	[48]
	LiCo_2O_4	142/84	4.1	344	[49]
Olivine	LiFePO_4	170/165	3.4	561	[50]
	LiMnPO_4	71/168	3.8	638	[51]
	LiCoPO_4	167/125	4.2	525	[52]
Tavorite	LiFeSO_4F	51/120	3.7	444	[53]
	LiVPO_4F	156/129	4.2	548	[54]

Table 2. Comparison of theoretical and experimental capacity of the major cathode materials and their average operational cell voltage.

However, the operational cell voltage is relatively lower than the spinel materials and some of the olivine phases. The energy density of Li_2MnO_3 , NCA, and NMC based phases is higher than other cathode materials. Apparently, it is seen from **Figure 3** that the spinel structure materials should exhibit higher power density than layer and olivine phases since it displays higher ionic diffusivity and conductivity as a function of lithium content as well as temperature. Nonetheless, particle morphologies play a crucial role in the power density and cycling stability of a battery. Three different types of particle morphologies are depicted in **Figure 4** as an example. It should be noted that each type of particle morphology has some inherent advantages and disadvantages for a particular material. It is well known that the spherical dense particle morphology (**Figure 4a**) is beneficial for the long-term cycling of layer structure materials with liquid electrolyte (LE). On the other hand, the nanometer-thick plate-like particle (**Figure 4b**) is good for olivine materials as they exhibit very low ionic and electronic properties transport (see **Figure 3** and **Table 1**). Rodlike particle morphologies (**Figure 4c**) of spinel materials are advantages for achieving high power densities. It is worth mentioning that the operational scenario of ASSB is very different than the conventional LE-based batteries. Unlike LE-based batteries, in SSBs, the solid electrolyte cannot penetrate inside the secondary particles as shown in the schematic (**Figure 4d-f**). Therefore, high power SSB cannot be achieved with a spherical particle in which ionic diffusion length would be longer and all particles might not be completely ionically wired. Submicron cathode particles (single crystals) are highly desirable for high performances SSB. Details are discussed in section 3 for requirements of cathode particles and the fabrication of composite electrodes for high-performance ASSB.

2.4. Suitability for solid-state battery

One of the major advantages of SSBs are the safe use of high voltage cathode materials (e. g. LMNO, LRM, and LCoP) which are not feasible in conventional

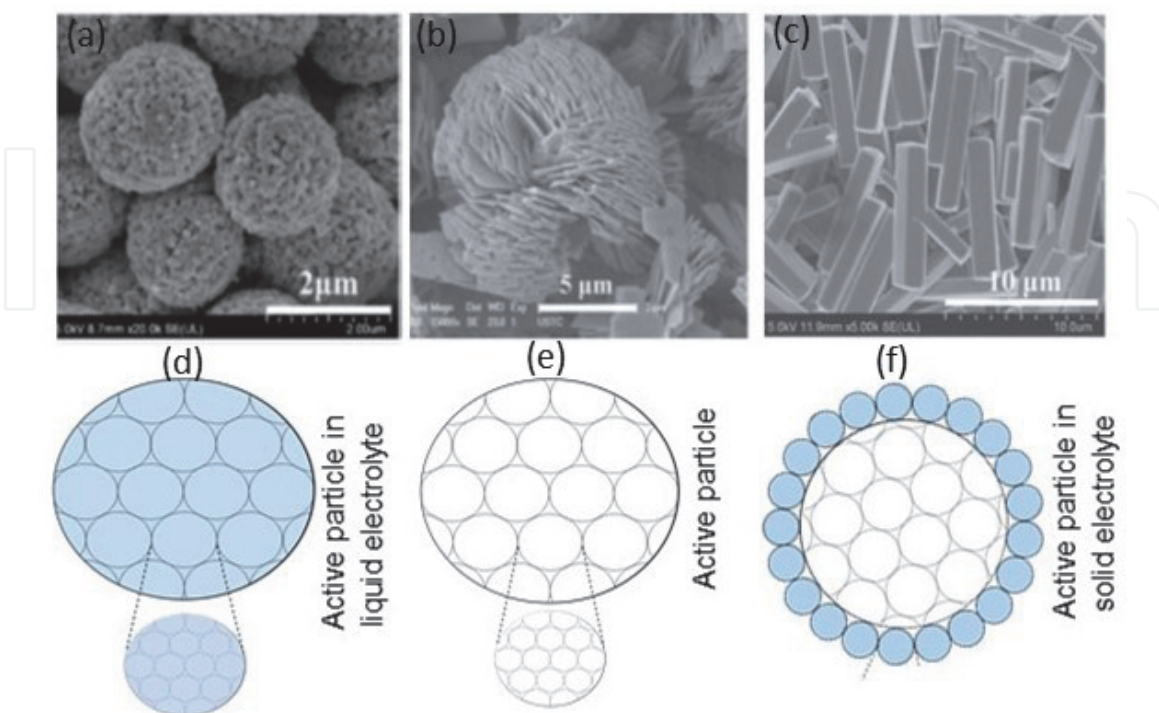
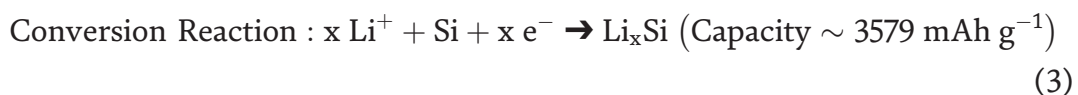
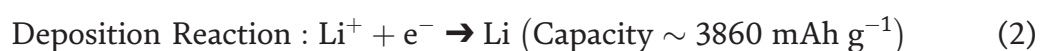


Figure 4. Particle morphologies of cathode materials (a-c) adapted from the references [55–57] and schematics showing the scenario of liquid and solid electrolytes for ionically wiring of cathode spherical particle (d-f).

liquid electrolytes due to their limited electrochemical stability window. Thus, SSBs are expected to provide a high energy density at the system level. However, the loose interfacial contact of oxide-based cathode and electrolyte (e. g. NMC/garnet-type electrolyte) creates a severe problem for cell voltage polarization and at room and low temperatures. In addition, a recent report has shown that solid electrolytes (SE) have instability issues while in direct contact with high voltage cathode materials [55]. In such a scenario, one sustainable solution might be the formation of a protective surface coating on cathode materials which would require stabilizing the cathode materials and SE interface by suppressing the possible oxidative reactions in the SSB. Furthermore, the primary cathode particles in the form of single crystals would be more beneficial for SSB than the secondary particles either in spherical or rod-like shapes. Unlike primary nanoparticles, the sphere of secondary particle has many separations or semi-separation regions between neighboring primary particles which is detrimental for SSB operation. Thus, single crystal cathodes are advantageous for use in SSBs because of their good crystallinity, high reaction homogeneity, mechanical strength, and better structural and thermal stability. All these salient features can remarkably improve the electrochemical performance and safety of the SSB.

3. Anode materials and designs for SSB

Anode materials can be broadly classified into three major types based on the mechanism of ion storage and electrochemical reactions occurring within the material [58]. The most common and prevalent type of anode material is the intercalation anode (**Figure 5a**) [59–61]. These materials typically possess layered structure into which Li-ion can reversibly insert (intercalate) during cycling of the battery [62]. Graphite, like several other materials (viz. LTO [63, 64], TNO [65]) is an intercalation type anode material. Conventional Li-ion batteries employ graphite as the anode material for hosting Li- ions for reversible intercalation and storage of electrochemical energy. Graphite has a theoretical capacity of 372 mAh g^{-1} which is higher than most cathode materials making it suitable as an anode material [66]. Graphite has demonstrated high coulombic efficiency and cycling performance making it ubiquitous in secondary lithium-ion batteries. These materials typically possess lower theoretical capacities; however, they are generally more stable and efficient electrodes. Alternate anode materials can be of deposition or conversion type depending on whether the mobile ion is depositing directly as a metal or as an alloy of a component respectively [3, 58, 67]. Alkali metals (Li, Na, etc.) are examples of deposition type anodes and they possess high theoretical capacity and relatively lower redox potentials [68]. Conversion type materials typically form alloys with the mobile ion (viz. In, Se, Si, etc.) and these also possess high theoretical capacity [69]. The major drawback for the deposition and conversion type anode materials are the electro-chemo-mechanical stability which makes them harder to integrate into functional devices compared to intercalation-type anode materials. Overall, typical reactions for each anode type can be given as:



Solid-state batteries rely on transitioning to high-capacity anode materials of the deposition or conversion type in order to achieve the expected improvements in the

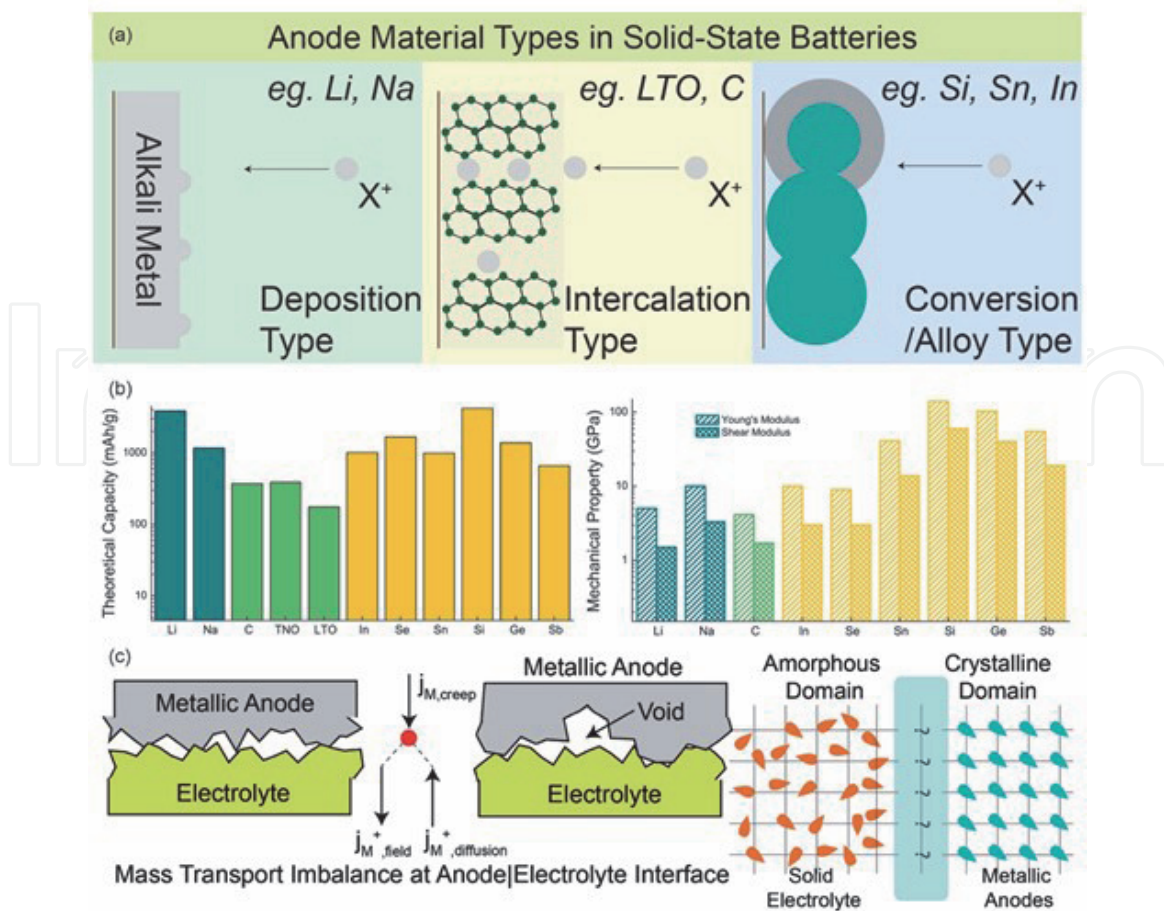


Figure 5. (a) Schematic diagram showing anode material type and operation mechanism. (b) Nominal capacities and mechanical properties of some common anode materials. (c) Schematic diagram highlighting the challenges with metallic anodes in terms of flux imbalance at the interface of solid electrolyte and the formation of reactive interphase at the electrode | electrolyte boundary.

energy density. A comparison of nominal capacity of several key deposition, intercalation and conversion type anode materials is provided in **Figure 5b**. It should be noted that the nominal capacities are plotted on a logarithmic scale. The comparison highlights that intercalation anode materials have an order of magnitude lower capacity compared to some conversion/deposition anode materials (375 mAh g^{-1} for graphite; 3860 mAh g^{-1} for Li, 3590 mAh g^{-1} for Si). Mechanical properties of materials are also of key interest for solid-state batteries in order to design solid electrolytes that can mitigate filament growth. Conversion type anode materials typically show higher Young's modulus and shear modulus compared to intercalation and deposition type anodes (**Figure 5b**). Solid electrolyte materials should ideally have shear modulus higher than the anode material in order to mitigate the growth of filaments as proposed by Monroe and Newman [70, 71]. It should be noted that the focus of anode studies with respect to solid-state batteries in the literature is primarily with lithium metal [3]. Relatively fewer reports on intercalation and conversion anode materials are reported and further work is anticipated in these material systems moving ahead.

The key challenges with deposition type anodes, and specifically Li metal will be discussed next. Controlling electrodeposition and electrodisolution morphology for Li metal is imperative to achieving stable solid-state batteries. Specifically, stable morphologies are required at the areal loading of $\sim 5 \text{ mAh cm}^{-2}$ of reversible cycling capacity at $\sim 5 \text{ mA cm}^{-2}$ plating current density with high coulombic efficiency is far from realization [11]. One major concern with lithium metal is the propensity

for filament growth leading to cell failure [72–74]. Filament formation can have significant negative impacts to rate performance, power density and coulombic efficiencies of SSBs. Filament growth typically stems from non-uniform deposition rate at the Li | SE interface. Interfacial kinetics heterogeneity at the Li metal solid electrolyte interface initiates several degradation pathways including filament formation limiting the stability and performance of solid-state batteries. In addition to growth of filaments, high rate electrodisolution from the Li metal can lead to formation of pores that can cause onset of failure [75]. A direct evidence of this was obtained from X-ray tomography measurements of Li | LLZO | Li symmetric cells (**Figure 5c**). Tracking pore evolution during cycling which showed clear cycling behavior (increase in porosity with stripping and decrease in porosity with plating). Mass transport within the Li metal is thus a key challenge and understanding creep and flow behavior of Li is necessary to tune the performance of the system. Interphase formation can also occur during integration of Li metal with solid-electrolytes [15]. Depending on the thermodynamic stability of the solid electrolyte material with lithium metal, three possible interphases can result. These are (i) thermodynamically and kinetically stable (no reaction @ Li | SE interface), (ii) Unstable (unmitigated reaction), and (iii) kinetically metastable (controlled reaction @ Li | SE interface) [3, 68, 73]. With the exception of few materials (viz. LLZO, LiPON), most solid electrolytes undergo reaction with Li metal due to inherent chemical and thermodynamic instability. For some materials, like NASICON-type LAGP and LATP materials as well as LPS thiophosphates, chemical and electrochemical reaction with Li metal leads to an unmitigated growth of an ionically insulating interphase coupled with volume expansion of the material [76–79]. This leads to higher impedances, local stress generation and inhomogeneous current distributions that can cause failure through filament formation, shorting or mechanical fractures. On the other hand, addition of stabilizing agents to the solid electrolyte or introduction of interlayers to these solid electrolytes can lead to formation of a meta-stable interphase that is a mixed ionic and electronic conductor leading to stable solid-state batteries.

Lithium metal stabilization is enabled by several strategies that can be broadly classified into: (i) electrolyte modification [84, 85] (ii) interface modification [86, 87] and (iii) operating parameter modification [80, 88, 89]. Electrolyte modification is afforded by additives that can promote the formation of kinetically metastable interphases [73]. For instance, LiI addition to LPS material in conjunction with microstructure control led to improvement of critical current density from $< 0.5 \text{ mA cm}^{-2}$ to $> 4 \text{ mA cm}^{-2}$. Similarly, halide addition to a range of solid electrolytes have shown improved performance in terms of ionic conductivity and critical current density. Interface modification is typically carried out by introducing the use of an interlayer barrier film at the anode | solid electrolyte interface. Atomic layer deposition of materials like Al_2O_3 , Si, $\text{Li}_x\text{Al}_{(2-x/3)}\text{O}$, LiXO_3 ($X = \text{Ta, Nb}$) has shown to improve the performance of lithium metal anodes [90–95]. However, typically the introduction of interlayers is carried out by cost-, time- and equipment-intensive processes that limit the large-scale deployment of such strategies. Another key strategy is modification of operating conditions primarily, temperature and pressure. Indeed, numerous studies have shown the importance of a critical stack pressure in order to mitigate the mass transport limitations within lithium metal by enhancing creep flow at higher pressures (**Figure 6a and b**) [81, 89, 96–98]. Overpotential at constant lithium stripping current (0.1 mA cm^{-2}) shows reversibly changing overpotentials with modification of the stack pressure. Similarly, overpotential as a function of applied current density shows a reduction of overpotential with increasing stack pressure. Silicon and indium-based anodes also show promising performance (**Figure 6d**) [82, 83]. In summary, anode materials

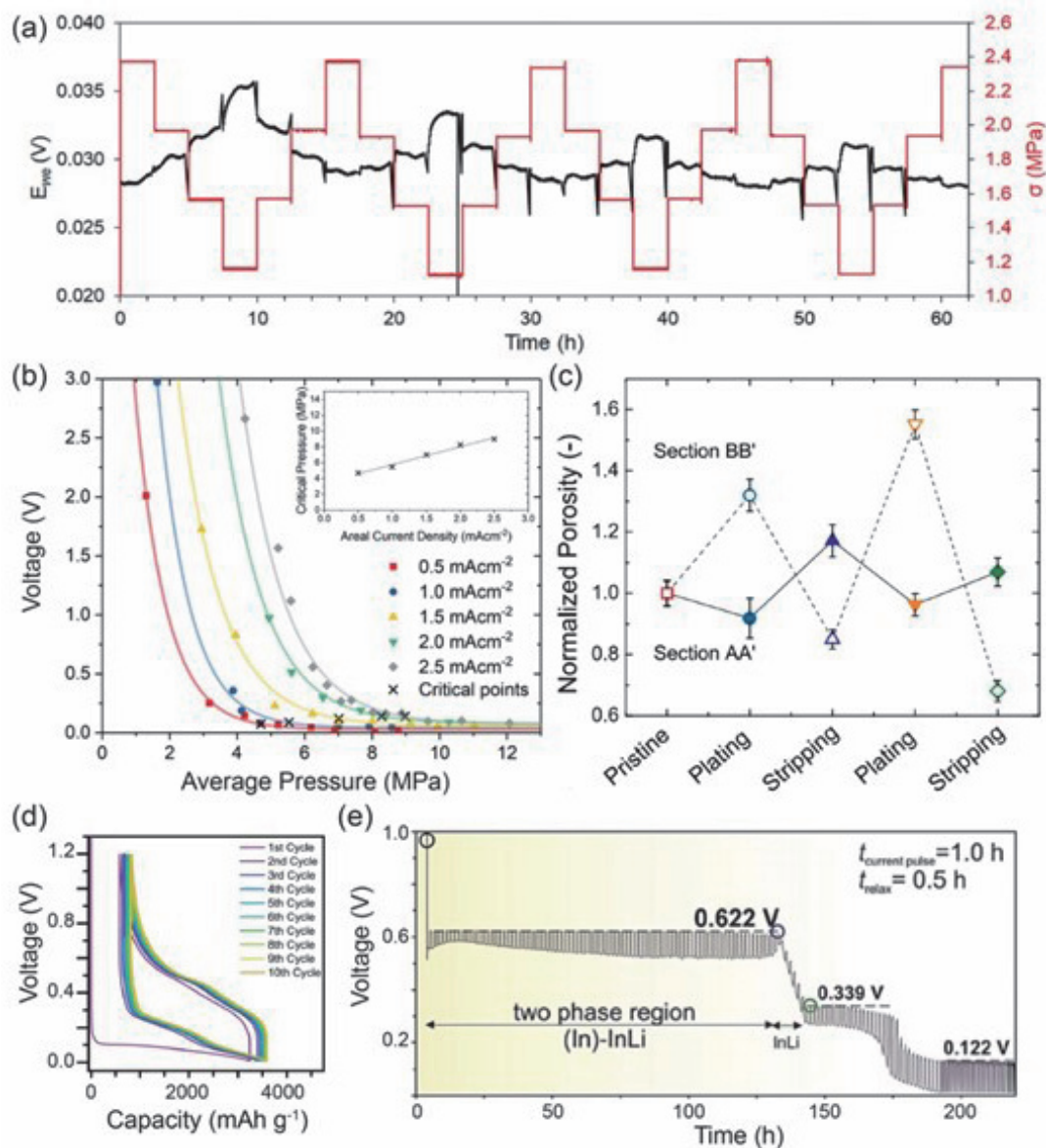


Figure 6.

Summary of key results from anode integration studies in solid state batteries. (a) Potential response of Li | LLZO | Li cell under constant current of 0.1 mA cm² under varying stack pressures. Reprinted with permission from [80]. (b) Influence of stack pressure on voltage increase for varying current densities for Na | β Alumina | Na cell with the inset showing the critical current density as a function of applied stack pressure. Reprinted with permission from [81]. (c) Porosity for two lithium metal electrodes as a function of cycling steps obtained from X-ray tomography measurements and machine learning segmentation. Reprinted with permission from [75]. (d) Silicon | LPS | Li cell cycling behavior. Silicon particles are spray coated on steel current collectors. Areal loading and current density for the test were 55 $\mu\text{g cm}^2$ and 0.06 mA cm² respectively. Reprinted with permission from [82]. (e) Potential profile during pulsed lithiation on In metal at 0.2 mA cm². LPS was used as the solid electrolyte. Reprinted with permission from [83].

for solid-state batteries need to provide high capacity with high-rate capabilities. Further work on stabilization of anodes under these conditions and demonstration of scalable integration approaches is required for deployment.

4. Solid electrolytes

Solid ion conductors have been synthesized in a wide range of chemistries (Figure 7) [99]. Currently, most promising electrolyte that have been investigated thoroughly are NASICON (LATP, LAGP) [100], Garnets (LLZO) [101] and Sulfides (LPS) [102]. However, each of these electrolytes have distinct limitations which are hindering their deployment in ASSBs. NASICONs have been widely investigated for

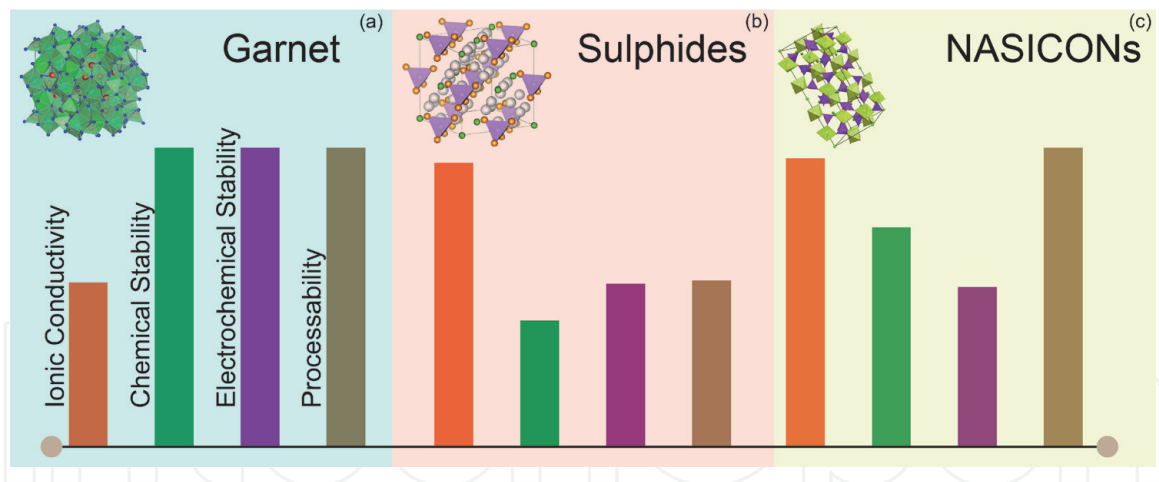


Figure 7. Schematic diagram highlighting the differences in properties of three major classes of solid electrolytes: (a) Garnet, (b) Sulphides, and (c) NASICONs.

not only Na-ion but also Li-ion all-solid-state batteries [103, 104]. $\text{Li}_{1.3}\text{Al}_{0.3}\text{Ti}_{1.7}(\text{PO}_4)_3$ (LATP) and $\text{Li}_{1.5}\text{Al}_{0.5}\text{Ge}_{1.5}(\text{PO}_4)_3$ (LAGP) are the two most popular NASICON electrolytes for Li-metal solid-state batteries. These electrolytes have high ionic conductivities ($\approx 10^{-3} \text{ S cm}^{-1}$) but suffer from stability issues as Ti^{4+} and Ge^{4+} undergo reduction in contact with Li metal anode [105–107]. First principles studies on these LATP and LAGP materials report operating voltage windows between 2.17 – 4.21V and 2.7 – 4.21V respectively. Garnet type electrolytes have garnered great attention due to their high electrochemical voltage window which enables high power density ASSB and enables long cycling life. However, garnet electrolytes have ionic conductivity one order of magnitude lower than LATP and LAGP. Garnet electrolytes also suffer from environmental instability which makes the processing of garnet type solid electrolyte cost intensive [108]. While a plethora of solid electrolyte classes have been explored over the years, the sodium superionic conductors or the NASICON class are slowly being re-examined for their high ionic conductivities, mechanical robustness and good chemical and electrochemical stabilities [109]. In particular, materials belonging to the NASICON family with phosphate anions are being extensively explored as potential electrolytes and cathode materials for Li, Na, and Mg-ion batteries owing to their high ionic conductivity, thermal and environmental stability [110]. The NASICON type $\text{Na}_{1+x}\text{Zr}_2\text{Si}_x\text{P}_{3-x}\text{O}_{12}$ ($0 \leq x \leq 3$) is a promising electrolyte material providing high ionic conductivity ($10^{-4} \text{ S cm}^{-1}$) at room temperature owing to the facile 3D ion conducting pathways. The general formula for these NASICON type materials is $\text{AM}_1\text{M}_2(\text{PO}_4)_3$ where A can be a monovalent cation Li^+ , Na^+ , K^+ , Rb^+ , Cs^+ , Ag^+ , Cu^+ , H^+ , H_3O^+ , NH_4^+ , or a divalent cation such as Mg^{2+} , Ca^{2+} , Sr^{2+} , Ba^{2+} , Pb^{2+} , Cd^{2+} , Zn^{2+} , Mn^{2+} , Fe^{2+} , Co^{2+} , Ni^{2+} or Cu^{2+} or it can also be vacant. M1 and M2 can be filled with di-, tri-, tetra- or pentavalent transition metal ions within the boundaries of charge balance. NASICONs can crystallize in three different crystal structures, based on the synthesis method, annealing temperature and choice of A, M1 and M2 resulting in α , β and γ -NASICON. Of these, γ -NASICON has the highest symmetry with $R\bar{3}C$ space group which is highly suitable for achieving high ionic conductivities. It is important to explore the possibility of Na-based NASICON materials to be able to conduct Li-ions as well.

Solid electrolytes have limited ionic conductivity at atmospheric temperatures which inhibits the rate capability of ASSB for practical applications (see Table 3). Ion transport in polymer electrolyte happens by the complexation of oxides while in inorganic electrolytes, it happens across the crystal lattice sites [111, 112]. Ion transport depends on the available lattice sites and activation barrier for hopping

from one lattice to other. Investigation on increasing available lattice sites for ion transport should be carried out for improving ion-transport. Garnet structures can be synthesized for different cubic structures to improve ion-conductivity. Sulfides have shown highest ionic conductivity among solid electrolytes but have major issues with sensitivity ambient environment since it produces H₂S when exposed to humidity. Low bending stiffness of ceramic electrolytes are hindering the processing with roll-to-roll manufacturing. Polymers can be easily processed but they don't have very high ionic conductivity (see **Table 3**). Thus, composite electrolytes can be one of the solutions to this conundrum.

Solid electrolyte must be chemically and electrochemically stable with the anode and cathode material at the operating potentials. Thermodynamic calculations based on the phase equilibria at the oxidation and reduction potential of

Type	Materials	Conductivity (S cm ⁻¹)	Advantages	Disadvantages
Oxide	Perovskite Li _{3.3} La _{0.56} TiO ₃ NASICON LiTi ₂ (PO ₄) ₃ LISICON Li ₁₄ Zn(GeO ₄) ₄ And garnet Li ₇ La ₃ Zr ₃ O ₁₂	10 ⁻⁵ to 10 ⁻³	<ul style="list-style-type: none"> • High chemical and electrochemical stability • High mechanical strength • High electrochemical oxidation voltage 	<ul style="list-style-type: none"> • Non-flexible • Expensive large-scale production
Sulfide	Li ₂ S-P ₂ S ₅ Li ₂ S-P ₂ S ₅ -MS _x	10 ⁻⁷ to 10 ⁻³	<ul style="list-style-type: none"> • High conductivity • Good mechanical strength and mechanical flexibility • Low grain-boundary resistance 	<ul style="list-style-type: none"> • Low oxidation stability • Sensitive to moisture • Poor compatibility with cathode material
Hydride	LiBH ₄ , LiBH ₄ -LiX (X = Cl, Br or I), LiBH ₄ -LiNH ₂ , LiNH ₂ Li ₃ AlH ₆ and Li ₂ NH	10 ⁻⁷ to 10 ⁻⁴	<ul style="list-style-type: none"> • Low grain-boundary resistance • Stable with lithium metal • Good mechanical strength and mechanical flexibility 	<ul style="list-style-type: none"> • Sensitive to moisture • Poor compatibility with cathode materials
Halide	Spinel Li ₂ ZnI ₄ and antiperovskite Li ₃ OCl	10 ⁻⁸ to 10 ⁻⁵	<ul style="list-style-type: none"> • Stable with lithium metal • Good mechanical strength and mechanical flexibility 	<ul style="list-style-type: none"> • Sensitive to moisture • Low oxidation voltage • Low conductivity
Borate and phosphate	Li ₂ B ₄ O ₇ , Li ₃ PO ₄ and Li ₂ O-B ₂ O ₃ -P ₂ O ₅	10 ⁻⁷ to 10 ⁻⁶	<ul style="list-style-type: none"> • Facile manufacturing process • Good manufacturing reproducibility • Good durability 	<ul style="list-style-type: none"> • Relatively low conductivity
Thin film	LiPON	10 ⁻⁶	<ul style="list-style-type: none"> • Stable with lithium metal • Stable with cathode materials 	<ul style="list-style-type: none"> • Expensive large-scale production
Polymer	PEO	10 ⁻⁴	<ul style="list-style-type: none"> • Stable with lithium metal • Flexible • Easy to produce a large area membrane • Low shear modulus 	<ul style="list-style-type: none"> • Limited thermal stability • Low oxidation voltage (<4 V)

Table 3.
Solid state electrolyte material for All-Solid-State Lithium Ion batteries.

Electrolyte	Reduction potential (vs Li)	Oxidation potential (vs Li)
Li ₂ S	-	2.01
LGPS	1.71	2.14
Li _{3.25} Ge _{0.25} P _{0.75} S ₄	1.71	2.14
Li ₃ PS ₄	1.71	2.31
Li ₄ GeS ₄	1.62	2.14
Li ₇ P ₃ S ₁₁	2.28	2.31
Li ₆ PS ₅ Cl	1.71	2.01
Li ₇ P ₂ S ₈ I	1.71	2.31
LiPON	0.68	2.63
LLZO	0.05	2.92
LLTO	1.75	3.71
LATP	2.17	4.21
LAGP	2.7	4.27
LISICON	1.44	3.39

Table 4.
 Oxidation and reduction potential of well-known solid electrolytes against Li/Li+.

well-known electrolytes showed that no electrolyte is simultaneously stable at both reductive potential of 0 V (vs Li) at the negative electrode and at typical positive potential of 4 V [113]. That's why chemically and electrochemically stable and lithium ion conducting interphase must be formed as depicted in the **Figure 7**. From the first principle calculation, reduction and oxidation potential of well know solid electrolytes are given in the **Table 4**.

5. Full cell integration

Material families that can meet ion transport criteria comparable to the state-of-the-art liquid electrolytes have been identified for solid ion conductors. Integration of these materials into a high-performance battery stack is still far from realization. The primary limitation in this regard is the lack of fundamental understanding of the interplay between charge transfer kinetics and mass transport within the system, specifically at the electrode | electrolyte interfaces in addition to other challenges (**Figure 8a**). Typical implementation of lab-scale solid-state batteries is not in traditional coin-cell or pouch-cell formats. Solid-state batteries are typically operated in “pressure cells” that encase the cell system in a container on which a mechanical load is applied (**Figure 8b**) in addition to temperature. Generally, SSBs are reported to function at operating pressures of >100 MPa and elevated temperatures (>50 °C). A quick survey of the reported SSB performance shows that the achieved specific energy and power density of SSBs fall short of required metrics of operations for SSBs of >400 Wh/kg gravimetric energy density and >200 W/kg power density (**Figure 8c**) [11]. Janek et al. have carried out extensive work to understand and decouple the influence of interphase formation and its impact on cycling of SSBs [117, 118]. Typical SSB cycling performance for sulphide based SSBs is depicted in **Figure 8d** [114]. The galvanostatic charge-discharge curves of NMC-811 | Li-In cells with LPS solid electrolyte (separator, catholyte: 30 %, active material: 70 %). SSB cell shows a large first cycle irreversibility (~30 %) compared to an

analogous conventional cell ($\sim 15\%$). Subsequent rate testing shows strong capacity loss at high C-rates with 0 mAh g^{-1} at 1C (**Figure 8d**). Subsequent long-term cycling at 0.1 C shows a strong capacity fade (1-2% each cycle) that is not observed for the conventional cell. The origin of this behavior is identified as a resistive layer formed on the cathode at the high charging voltages which is validated by in situ impedance spectroscopy, SEM and XPS measurements. NCA cathode material with LPSCl solid electrolyte and Li metal anode was investigated in full cells at 5 MPa stack pressure [88]. LNO-coated NCA shows a first cycle irreversibility similar to NMC materials with subsequent cycles showing higher coulombic efficiency ($\sim 98\%$). 80% retention over 200 cycle was observed for this cell at the 5 MPa stack operating pressure and $\sim 3.5 \text{ mg cm}^{-2}$ active material loading. The results suggest optimization of the operating conditions (pressure, temperatures) in order to mitigate the formation of filaments and extend SSB lifetimes. Similar studies have been carried out for different cathode and solid electrolyte material combinations that highlight the need of tailoring cathode microstructure, interfaces, reactivity as well as mechanics of the composite cathode. Dixit et al. investigated LFP based cathode composites in conjunction with hybrid solid electrolytes (PEO-LLZO) with varying mechanical properties (**Figure 8e**) [115]. The results indicated that solid electrolyte with higher adhesion properties at the interface shows improved performance due to improved wetting and contact with the cathode. SSB micro-batteries are also investigated as a potential architecture to maximize areal capacity and electrochemically active surface areas for niche applications. MoOS_2 cathode material in conjunction with PVDF-based solid electrolyte and mesoporous carbon anode was used to fabricate 3D micro-batteries using thin-film coating processes [116]. The results from this study showed improved areal capacity of over an order of

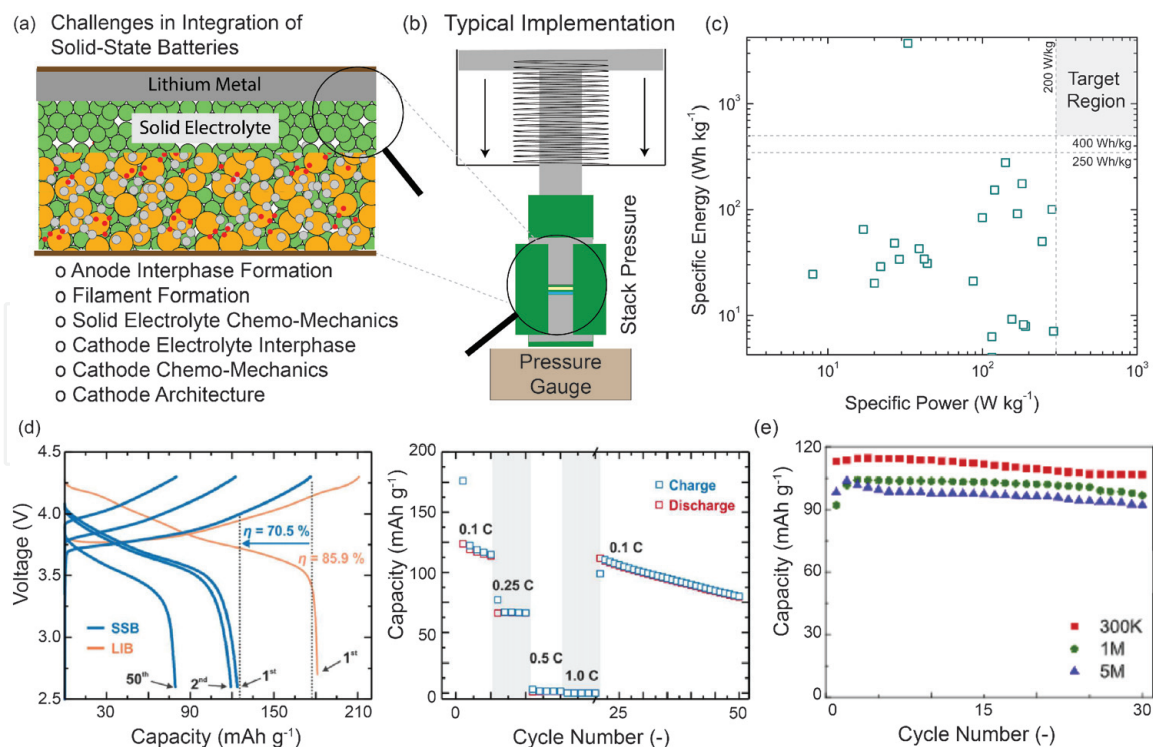


Figure 8.

(a) Schematic diagram highlighting the challenges in integration of all solid-state batteries. (b) Schematic diagram of a typical implementation of a solid-state battery cell. (c) Summary of experimentally reported energy and power density of solid-state batteries. Note that the target performance region for solid state batteries is shaded. (d) Polarization curves and rate performance of NMC-811 | Li-In cells with LPS solid electrolyte (separator, catholyte: 30%, active material: 70%). Reprinted with permission from [114]. (e) Cycling performance of LFP | PEO-LLZO | Li cells for hybrid solid electrolytes with three different molecular weights 300K, 1M and 500 K. Reprinted with permission from [115].

magnitude for 3D micro-battery compared to a traditional 2D architecture processed identically.

Recently, Dixit et al. carried out a numerical study on investigation on impact of cathode architecture on the energy density of solid-state batteries [14]. They identified a necessity for a large variation in particle size of cathode components in order to achieve higher density composite cathodes as well as to achieve high contact area between the solid-electrolyte and cathode active material. Additionally, the influence of excess anode material to the resultant cell-level energy density was investigated (**Figure 9a–c**). Transitioning to low/no- excess anodes systems can provide significant improvements in terms of cell-level energy density. Dense solid electrolytes (\sim LLZO) result in high volumetric energy density while low-density solid electrolyte (\sim PEO) in conjunction with high voltage/capacity cathode materials. Limited demonstrations of completely anode-free cells are observed in literature. Cycling of an in-situ formed Li anode in a NCA | LLZO anode free cell is highlighted here (**Figure 9d and e**). The investigated anode free system shows typically low cathode utilization due to unoptimized cathode architecture with highly reversible cycling (coulombic efficiencies \sim 100%) over 50 cycles [119]. It should be noted that due to changes in “accessible” lithium, certain discharge cycles show higher capacities than the corresponding charge cycle. Another important consideration in solid-state battery architecture is the concept of bipolar stacking. The use of solid electrolyte mitigates the shorting and electrolyte leaking in unit cells allowing for series stacking and reduction of inactive materials in the cell (packaging, sealing, conductor elements). This can lead to improvement in both gravimetric energy density as well power density due to reduction in inactive materials as well as overall resistance of the modules. Initial results with excess-area stainless steel

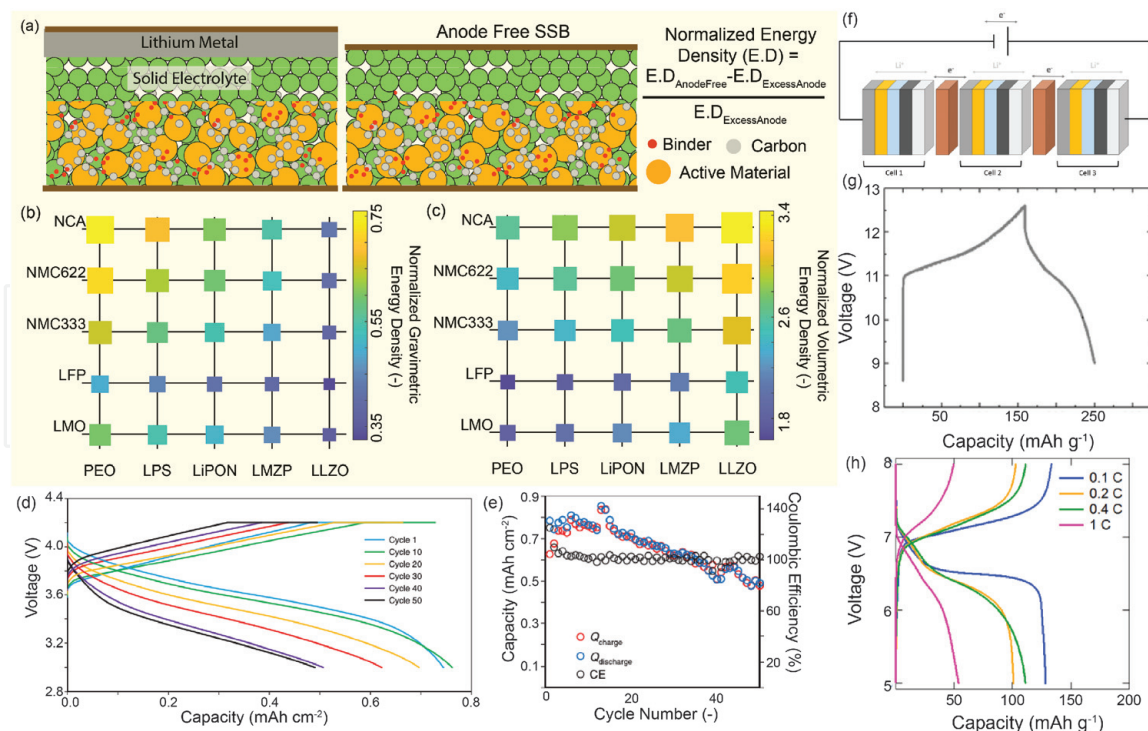


Figure 9. (a) Schematic diagram showing the differences in SSBs with and without anode incorporated in the system. Effect of transitioning to a no-excess anode system from a 100% excess anode system on (b) gravimetric energy density and (c) volumetric energy density for a range of material combinations. Reprinted with permission from [14]. (d–e) Cycling performance of an anode free NCA|LLZO cell after initial charging cycle at 0.05 mA cm². Stack pressure of 4 MPa was used for the tests. Reprinted with permission from [119]. (f) Schematic diagram showing bipolar stacking of solid-state batteries. Typical polarization curve for bipolar stacked SSBs with (g) NMC and (h) LFP based cathode materials. Reproduced with permission from [120, 121].

current collector as a bipolar plate shows promising polarization profiles for NMC622 as well as LFP -based SSBs with polymer based solid electrolytes [120–123]. Subsequent investigations into materials, architectures and cell design for bipolar stacking needs to be carried out for high energy and power density SSBs.

6. Perspective and outlook

Battery research at present is at a stage where SSB technology can either redefine the next generation of batteries or fizzle out without making an impact. The key difference between the two scenarios is whether the underlying challenges can be systematically mitigated or not. With more commercial enterprises investing heavily into SSB research, there is momentum slowly building to propel and position SSBs as the batteries of the future. Success of SSBs would depend upon the following factors: (i) improving the interfacial issues, (ii) developing unique processing capabilities while minimizing cost, (iii) addressing cell and pack level design challenges when integrating solid state components, and (iv) demonstrating performances exceeding that of advanced lithium-ion batteries. Some potential challenges and opportunities for SSBs include:

With the electric vehicle revolution driving up the demand for batteries that can deliver high energy density, can fast charge, have long cycle and calendar life while maintaining low manufacturing costs, there is definite potential for SSBs to play a major role in achieving these goals. Moreover, the US Department of Energy's target goal for EV batteries include (i) of reducing battery cost to $< \$100/\text{kWh}$ and ultimately to $< \$80/\text{kWh}$, (ii) increasing the range of electric vehicles to 300 miles and (iii) decreasing charge time to 15 minutes or less. A full solid-state battery that can meet these targets that are set for electric vehicles in the next decade is an ambitious endeavor especially when the best anode, cathode, and electrolyte chemistries for such an SSB are not obvious at present.

Urban air mobility is a rapidly pursued avenue that could redefine transportation as we know it. Conventional liquid electrolyte-based batteries are subjected to increasingly stringent safety requirements for use in operation of auxiliary electronics on present day aircraft platforms. Applications with demanding duty cycles such as electric vehicle take off and lift (EVTOL) platforms require batteries that can operate at extreme temperature gradients while being subjected to a multitude of mechanical stresses during operation. SSBs with their safety and energy density advantages are uniquely positioned to be the go-to batteries for such applications. Exploring SSBs for such applications would require coordinated efforts between industrial players and research institutes to initially define the performance requirements for such platforms followed by systematic material and engineering efforts to address the challenges.

- i. Extreme environment batteries are a niche yet rapidly growing application due to the increasing public interest into commercial low-earth orbit and interplanetary travel. Certain terrestrial, upper altitude and space applications necessitate secondary energy storage technologies that can function under a very wide modality of extreme environmental conditions including but not limited to temperature, pressure, radiation loads, and mechanical loads. With some present day SSBs operating efficiently at elevated temperatures when compared to the room temperature performance, this presents a unique opportunity for deploying SSBs in these applications. Development of stable, safe, and durable energy storage technologies can have a transformational impact on the application sectors

which can include orbital satellites, outer planetary/deep-space probes, land rovers, polar vehicles/end stations, among others.

- ii. As an intermediate step, a less-demanding end use application such as SSBs for portable/wearable electronics can be pursued, however, this would risk diverting the focus of the battery R&D community from the biggest projected market for next generation battery systems – electric vehicles and grid storage.

7. Conclusion

In summary, despite the challenges, solid-state batteries have great potential for implementation in applications that demand high-energy and safe batteries. Successful deployment of practical SSBs is contingent on addressing the underlying challenges related to materials, processing, and cell engineering. Through this chapter, we have discussed the key issues pertaining to the specific SSB cell components – cathode, solid electrolyte and anode and their interfaces. We envision that our perspectives and outlook discussed in this chapter encourages the readers and inspires solutions that would lead to the eventual practical realization and wide commercial deployment of energy dense solid state battery systems.

Acknowledgements


This work at the Oak Ridge National Laboratory, managed by UT Battelle, LLC, for the U.S. Department of Energy (DOE) under Contract No. DE-AC05-00-OR22725, was sponsored by the Laboratory Directed Research and Development Program at Oak Ridge National Laboratory.

Author details

Marm Dixit, Nitin Muralidharan, Anand Parejiya, Ruhul Amin*, Rachid Essehli and Ilias Belharouak*
Electrification and Energy Infrastructure Division, Oak Ridge National Laboratory, Oak Ridge, Tennessee, USA

*Address all correspondence to: aminr@ornl.gov;

IntechOpen

© 2021 The Author(s). Licensee IntechOpen. This chapter is distributed under the terms of the Creative Commons Attribution License (<http://creativecommons.org/licenses/by/3.0>), which permits unrestricted use, distribution, and reproduction in any medium, provided the original work is properly cited. 

References

- [1] The. *Glob. EV Outlook 2020* **2020**.
- [2] Janek, et al. *Nat. Energy* **2016**, *1*, 16141.
- [3] Hatzell, et al. *ACS Energy Lett.* **2020**, *5*, 922–934.
- [4] Wood, et al. *ACS Energy Lett.* **2017**, *2* (3), 664–672.
- [5] Xiao, et al. *Nat. Energy* **2020**, *5* (8), 561–568.
- [6] Fan, et al. *Adv. Energy Mater.* **2018**, *1702657*, 1–31.
- [7] Bachman, et al. *Chem. Rev.* **2016**, *116* (1), 140–162.
- [8] Løvvik, et al. **2019**.
- [9] Mai, et al. *Natl. Renew. Energy Lab.* **2018**, 151.
- [10] Kapustin, et al. *Energy Policy* **2020**, *137* (November 2019), 111103.
- [11] Randau, et al. *Nat. Energy* **2020**, *5* (3), 259–270.
- [12] Shen, et al. *J. Electrochem. Soc.* **2019**, *166* (14), A3182–A3188.
- [13] Dixit, et al. *ACS Appl. Mater. Interfaces* **2019**, *11* (48), 45087–45097.
- [14] Dixit, et al. *Energy Storage Mater.* **2021**.
- [15] Banerjee, et al. *Chem. Rev.* **2020**, *120* (14), 6878–6933.
- [16] Wang, et al. *J. Am. Chem. Soc.* **2018**, *140* (1), 250–257.
- [17] Whittingham. *Materials science and technology*; Elsevier Science, 2012.
- [18] Thompson. *Phys. Rev. Lett.* **1975**, *35* (26), 1786–1789.
- [19] Gamble, et al. *Science* (80-.). **1971**, *174* (4008), 493–497.
- [20] Aronson, et al. *The Journal of Chemical Physics*. NUMBER I I September 18, 1968, pp 470–471.
- [21] Whittingham. *Science* (80-.). **1976**, *192* (4244), 1126–1127.
- [22] Dyer, et al. *Science* (80-.). **2013**, *340* (6134), 847–852.
- [23] Islam, et al. *Chemical Society Reviews*. Royal Society of Chemistry January 7, 2014, pp 185–204.
- [24] Amin, et al. *Electrochem. Solid-State Lett.* **2007**, *10* (1), A13.
- [25] Amin, et al. *J. Electrochem. Soc.* **2016**, *163* (8), A1512–A1517.
- [26] Amin, et al. *J. Electrochem. Soc.* **2015**, *162* (7), A1163–A1169.
- [27] Amin, et al. *J. Power Sources* **2017**, *348*, 318–325.
- [28] Amin, et al. *J. Power Sources* **2017**, *348*, 311–317.
- [29] Wu, et al. *J. Electrochem. Soc.* **2012**, *159* (4), A438–A444.
- [30] Hao. City University of Hong Kong, 2010.
- [31] Seid, et al. *Phys. Chem. Chem. Phys.* **2013**, *15* (45), 19790–19798.
- [32] Li, et al. *Energy Environ. Sci.* **2014**, *7* (2), 768–778.
- [33] Saadoun, et al. *J. Solid State Chem.* **1998**, *136* (1), 8–15.
- [34] Montoro, et al. *Electrochim. Acta* **2004**, *49* (19), 3243–3249.

- [35] Sivonxay, et al. *Electrochim. Acta* **2020**, 331, 135344.
- [36] Tritsarlis, et al. *J. Phys. Chem. C* **2012**, 116 (42), 22212–22216.
- [37] Wu, et al. *Ceram. Int.* **2019**, 45 (4), 5072–5079.
- [38] Kim, et al. *Journal of Alloys and Compounds*. Elsevier March 4, 2010, pp L87–L90.
- [39] Zhang, et al. *ACS Appl. Mater. Interfaces* **2014**, 6 (20), 17965–17973.
- [40] Che, et al. *J. Electrochem. Soc.* **1997**, 144 (12), 4296–4302.
- [41] Cho, et al. *Angew. Chemie - Int. Ed.* **2003**, 42 (14), 1618–1621.
- [42] Ohzuku, et al. *J. Electrochem. Soc.* **1993**, 140 (7), 1862–1870.
- [43] Bruce, et al. In *Journal of Materials Chemistry*; Royal Society of Chemistry, 1999; Vol. 9, pp 193–198.
- [44] Tu, et al. *Electrochim. Acta* **2006**, 51 (28), 6456–6462.
- [45] Lin, et al. *Nat. Commun.* **2014**, 5 (1), 3529.
- [46] Wang, et al. *Adv. Energy Mater.* **2013**, 3 (10), 1358–1367.
- [47] Lee, et al. *Nano Lett.* **2014**, 14 (2), 993–999.
- [48] Nisar, et al. *J. Power Sources* **2018**, 396, 774–781.
- [49] Choi, et al. *J. Electrochem. Soc.* **2002**, 149 (2), A162.
- [50] Yamada, et al. *J. Electrochem. Soc.* **2001**, 148 (3), A224.
- [51] Choi, et al. *Nano Lett.* **2010**, 10 (8), 2799–2805.
- [52] Lloris, et al. *Electrochem. Solid-State Lett.* **2002**, 5 (10), A234.
- [53] Barker, et al. In *Journal of Power Sources*; Elsevier, 2005; Vol. 146, pp 516–520.
- [54] Sobkowiak, et al. *Chem. Mater.* **2013**, 25 (15), 3020–3029.
- [55] Guo, et al. *Electrochim. Acta* **2017**, 236, 171–179.
- [56] Ma, et al. *Angew. Chemie - Int. Ed.* **2016**, 55 (11), 3667–3671.
- [57] Wang, et al. *J. Power Sources* **2011**, 196 (23), 10176–10182.
- [58] Puthusseri, et al. *ACS Omega* **2018**, 3 (4), 4591–4601.
- [59] Parikh, et al. *J. Electrochem. Soc.* **2019**, 166 (14), A3377–A3383.
- [60] Wood, et al. *Energy Storage Mater.* **2020**, 29, 254–265.
- [61] Jaiser, et al. *J. Power Sources* **2016**, 318, 210–219.
- [62] Takami, et al. *J. Electrochem. Soc.* **2000**, 142 (2).
- [63] Nordh, et al. *ChemElectroChem* **2017**, 4 (10), 2683–2692.
- [64] Pfenninger, et al. *Adv. Funct. Mater.* **2018**, 28 (21), 1–8.
- [65] Lee, et al. *Sci. Rep.* **2017**, 7 (1), 1–13.
- [66] Asenbauer, et al. *Sustain. Energy Fuels* **2020**, 4 (11), 5387–5416.
- [67] El kharbachi, et al. *Solid State Ionics* **2018**, 317 (September 2017), 263–267.
- [68] Krauskopf, et al. *Chem. Rev.* **2020**.
- [69] Baggetto, et al. *Adv. Funct. Mater.* **2008**, 18 (7), 1057–1066.

- [70] Monroe, et al. *J. Electrochem. Soc.* **2003**, 150 (10), A1377–A1384.
- [71] Monroe, et al. *J. Electrochem. Soc.* **2005**, 152 (2), A396.
- [72] Shen, et al. *ACS Energy Lett.* **2018**, acsenergylett.8b00249.
- [73] Dixit, et al. *Matter* **2020**, 3 (6), 2138–2159.
- [74] Dixit, et al. *ACS Appl. Mater. Interfaces* **2018**, 11, 2022–2030.
- [75] Dixit, et al. *ACS Appl. Energy Mater.* **2020**, 3 (10), 9534–9542.
- [76] Lewis, et al. *ACS Energy Lett.* **2019**, 4, 591–599.
- [77] Albertus, et al. *ACS Energy Lett.* **2021**, 1399–1404.
- [78] Tippens, et al. *ACS Energy Lett.* **2019**, 4 (6), 1475–1483.
- [79] Lewis, et al. *Nat. Mater.* **2021**, c.
- [80] Wang, et al. *Joule* **2019**, 3 (9), 2165–2178.
- [81] Spencer Jolly, et al. *ACS Appl. Mater. Interfaces* **2020**, 12 (1), 678–685.
- [82] Ohta, et al. *ACS Appl. Energy Mater.* **2019**, 2 (10), 7005–7008.
- [83] Santhosha, et al. *Batter. Supercaps* **2019**, 2 (6), 524–529.
- [84] Bonnicks, et al. *J. Mater. Chem. A* **2019**, 7 (42), 24173–24179.
- [85] Singh, et al. *Chem. Mater.* **2020**.
- [86] Han, et al. *Nat. Mater.* **2017**, 16 (5), 572–579.
- [87] Liu, et al. *ACS Mater. Lett.* **2020**, 665–670.
- [88] Doux, et al. *Adv. Energy Mater.* **2020**, 10 (1).
- [89] Kasemchainan, et al. *Nat. Mater.* **2019**.
- [90] Han, et al. *Nat. Mater.* **2017**, 16 (5), 572–579.
- [91] Luo, et al. *J. Am. Chem. Soc.* **2016**, 138 (37), 12258–12262.
- [92] Gellert, et al. *J. Electrochem. Soc.* **2015**, 162 (4), A754–A759.
- [93] Xu, et al. *Joule* **2018**, 2 (10), 1991–2015.
- [94] Cao, et al. *Matter* **2020**, 3 (1), 57–94.
- [95] Cheng, et al. *Chem. Rev.* **2017**, 117 (15), 10403–10473.
- [96] Tu, et al. *Cell Reports Phys. Sci.* **2020**, 1 (7), 100106.
- [97] Qingsong, et al. **2019**, 1–38.
- [98] Zhang, et al. *Cell Reports Phys. Sci.* **2020**, 1 (2), 100012.
- [99] Manthiram, et al. *Nat. Rev. Mater.* **2017**, 2 (4).
- [100] Zheng, et al. *J. Power Sources* **2018**, 389 (April), 198–213.
- [101] Liu, et al. *J. Power Sources* **2018**, 389 (April), 120–134.
- [102] Lau, et al. *Adv. Energy Mater.* **2018**, 8 (27), 1–24.
- [103] Gao, et al. *Chem* **2018**, 4 (4), 833–844.
- [104] Mertens, et al. *Solid State Ionics* **2017**, 309 (July), 180–186.
- [105] Sun, et al. *J. Power Sources* **2020**, 471 (July), 1–9.
- [106] Meesala, et al. *J. Phys. Chem. C* **2018**, 122 (26), 14383–14389.

- [107] Wang, et al. *Electrochim. Acta* **2020**, 334, 1–8.
- [108] Xia, et al. *J. Am. Ceram. Soc.* **2017**, 100 (7), 2832–2839.
- [109] Xia, et al. *ACS Applied Mater. Interfaces* **2016**, 8 (8), 5335–5342.
- [110] Parejiya, et al. *ACS Energy Lett.* **2021**, 429–436.
- [111] Famprakis, et al. *Nat. Mater.* **2019**, 18 (12), 1278–1291.
- [112] Liu, et al. *Chem. - A Eur. J.* **2018**, 1–15.
- [113] Luntz, et al. *J. Phys. Chem. Lett.* **2015**, 6 (22), 4599–4604.
- [114] Koerver, et al. *Chem. Mater.* **2017**, 29 (13), 5574–5582.
- [115] Dixit, et al. *Joule* **2020**, 4 (1), 207–221.
- [116] Oudenhoven, et al. *Adv. Energy Mater.* **2011**, 1 (1), 10–33.
- [117] Neumann, et al. *ACS Appl. Mater. Interfaces* **2020**, 12 (8), 9277–9291.
- [118] Schmalzried, et al. *Ber. Bunsenges. Phys. Chem* **1998**, 102, 127–143.
- [119] Wang, et al. *Nat. Commun.* **2020**, 11 (1), 1–9.
- [120] Homann, et al. *ACS Appl. Energy Mater.* **2020**, 3 (4), 3162–3168.
- [121] Matsuo, et al. *Sci. Rep.* **2014**, 4, 1–5.
- [122] Gambe, et al. *Sci. Rep.* **2015**, 5, 10–13.
- [123] Liu, et al. *Adv. Sci.* **2020**, 7 (17), 1–13.